Electronic Supplementary Material (ESI) for Physical Chemistry Chemical Physics.
This journal is © the Owner Societies 2014

Supporting information

Table S1 The specific surface area (S_{BET}) pore volume (Vp), and average pore diameter of the samples at different milling speed and with different C_3N_4 loading.

Samples	ZnO		1%-C_3N_4@ZnO	3%-C_3N_4@ZnO			5%-C_3N_4@ZnO	7%-C_3N_4@ZnO
	Without milled	350 rpm	350 rpm	250 rpm	300 rpm	350 rpm	350 rpm	350 rpm
S_{BET} (m^2/g)	10.3	13.0	16.0	12.3	12.1	12.5	8.5	5.4
Pore volume (cm^3/g)	0.03	0.06	0.06	0.05	0.04	0.04	0.03	0.02
Average pore diameter (nm)	10.02	18.3	15.2	15.9	12.8	14.0	16.5	15.7

1. Morphology and size of the sample

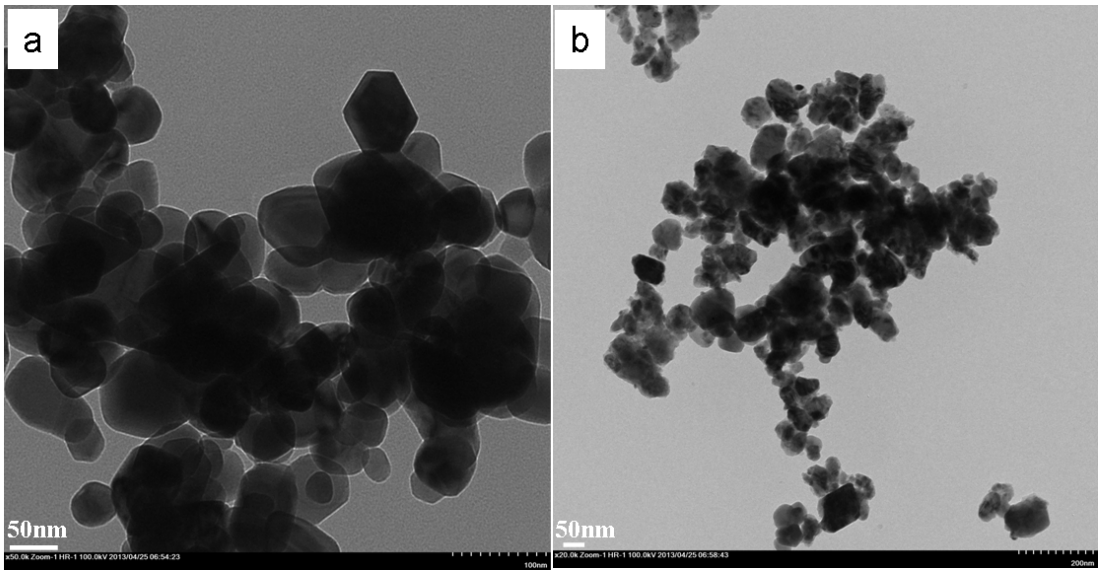

Fig.1 TEM image for （a）nano-ZnO (before milling), （b）g- C_3N_4@ZnO (milled)

Figure 1 shows the TEM image for nano-ZnO and g-C_3N_4@ZnO hybrid catalyst after ball milling process. The images show that the diameters of ZnO (Fig.1a) particles and g-C_3N_4@ZnO (Fig.1b) materials are about 20 nm.

2. FT-IR spectra

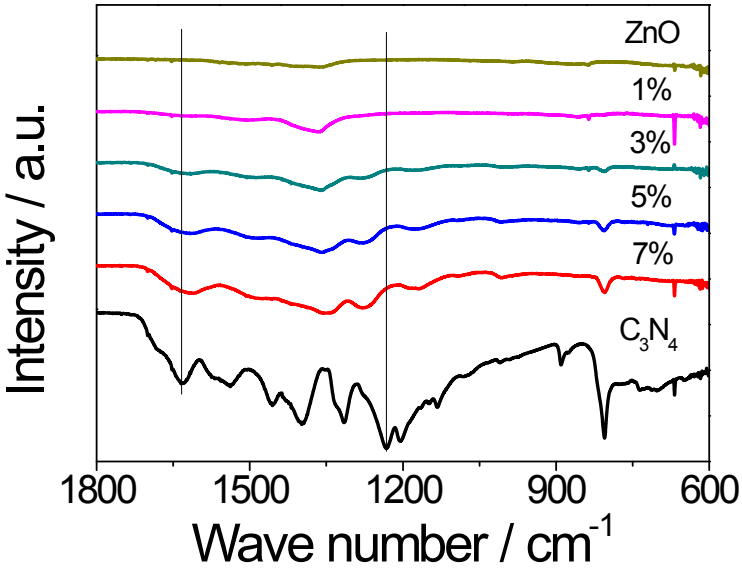

Fig.2 FT-IR spectra of C_3N_4, ZnO and C_3N_4@ZnO（A resolution of 0.5 cm^{-1}）

Fig.2 illustrates the FT-IR spectrum of C_3N_4, ZnO and g-C_3N_4@ZnO, respectively. The FT-IR spectra of the synthesized g-C_3N_4 are similar to the results reported previously. The absorption band near 1635 cm^{-1} is attributed to C–N stretching, while the three bands at 1240, 1320 and 1405 cm^{-1} are originate from aromatic C–N stretching. The band near 810 cm^{-1} is attributed to out-of plane bending modes of C–N heterocycles[1,2]. Abroad band near 3140 cm^{-1} corresponds to the stretching modes of terminal NH_2 or NH groups at the defect sites of the aromatic ring [3]. The FT-IR spectra of g-C_3N_4@ZnO photocatalysts are also similar to those of the main peaks of g-C_3N_4 wave-number. With the amount of doped g-C_3N_4 increasing, the absorbance band intensity of g-C_3N_4@ZnO is gradually increase, which indicts the formation of a composite between ZnO and C_3N_4. The stronger valence bond interaction between C_3N_4 and ZnO may be the key to enhance photocatalytic activity.

3. XRD patterns

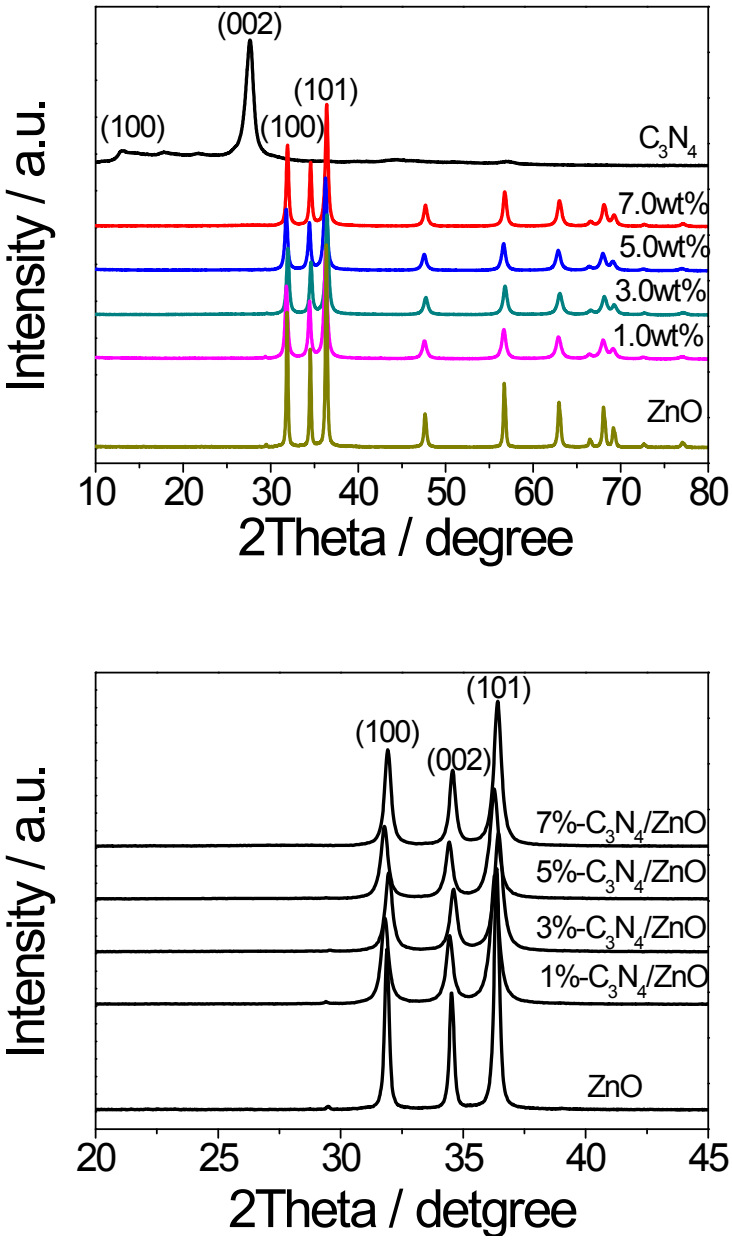

Fig.3 The enlarged XRD patterns of C_3N_4, ZnO and C_3N_4@ZnO hybrid composite

Fig.3 shows the XRD patterns of different photocatalysts. Two pronounced peaks were found in g-C_3N_4 at 27.4° and 13.1°, which can be indexed as (100) and (002) diffraction planes. The XRD peaks of the pure ZnO sample are in good agreement with the hexagonal wurtzite crystal phase of ZnO (JCPDS 65-3411). The diffraction peaks of g-C_3N_4 cannot be found owing to the corresponding intensity of C_3N_4 is

much lower than that of ZnO so that the changes of diffraction peaks of C_3N_4 are not obvious in the patterns. The same results were obtained in previous reports [4,5]. This illustrates that g-C_3N_4 is highly dispersed in the bulk phase of the catalyst. Furthermore, the XRD patterns reveal that the ZnO peak intensities decrease gradually with increasing g-C_3N_4 content in the composite. No other new crystal phases are found in Fig.3, demonstrating that the C_3N_4@ZnO sample presents a two-phase composition: C_3N_4 and ZnO.

4. Raman spectra

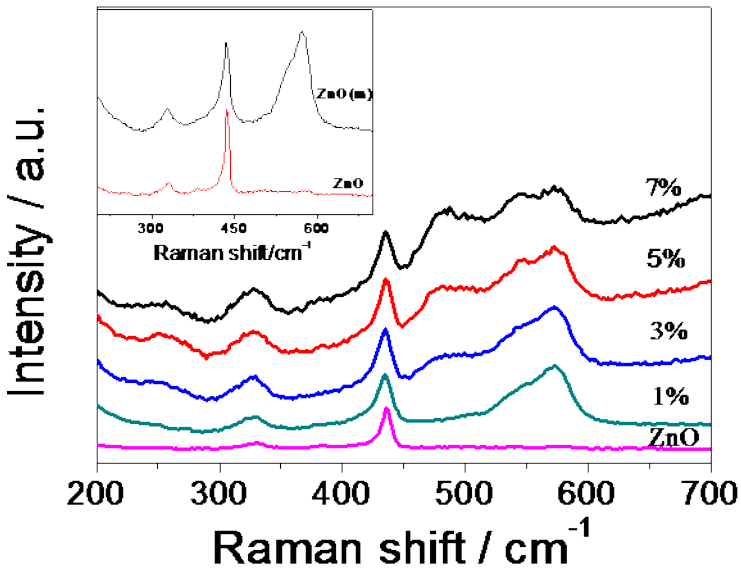

Fig.4 Raman spectra of g-C_3N_4@ZnO and pure ZnO. (Excitation wavelength: 514 nm)

higher inset: Characterization of the pure ZnO (raw material) and ZnO (milled)

Raman spectra were shown in Fig 4. Samples have four peaks (332.7 cm^{-1}, 386.2 cm^{-1}, 439.3 cm^{-1} and 583.5 cm^{-1}). Compared with pure ZnO, the peaks of g-C_3N_4@ZnO at 332.7 cm^{-1} and 583.5 cm^{-1} become strong, while the peak at of 386.2 cm^{-1} is not observed and that of 439.3 cm^{-1}does not change, which might be attributed to defects that formed in mechanical process. With the increasing amount of C_3N_4 in the catalyst, the peaks become wider, which imply the hybridism of C_3N_4 and ZnO.

5. Fluorescence emission spectra

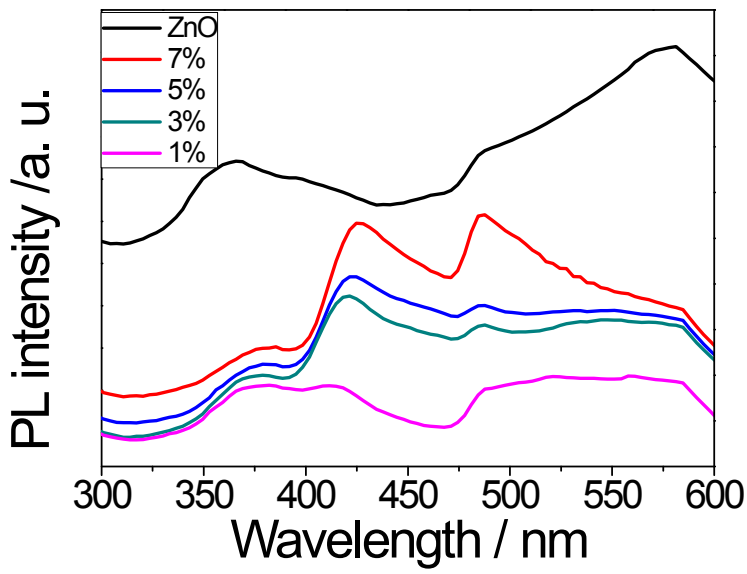

Fig.5 Fluorescence emission spectra of different samples (Excitation wavelength: 325 nm)

Photocatalysts generate electrons and holes after being activated by light, and recombination of some electrons and holes can release energy in the form of fluorescence emission. Lower fluorescence emission intensity implies lower electron–hole recombination rate [6]. Using an ultraviolet light with a 325 nm wavelength as the excitation source, the fluorescence emission spectra of ZnO hybridization with different contents of g-C_3N_4 are shown in Fig.5. ZnO has three peaks: UV emission peaks (380 nm), for free carrier interband recombination, blue light emitting (450 nm), for the transition of oxygen vacancy of shallow donor level to valence band, defect emission peaks (470~600nm), caused by the transition of valence band. ZnO has the greatest relative intensity of emission spectra, which means that electrons and holes of ZnO are easy to recombine. The relative intensity of the g-C_3N_4@ZnO is lower than that of ZnO, it is clear that hybridization is helpful to inhibit the recombination of electrons and holes and improve the photocatalytic activity. With the increasing amount of C_3N_4 content from 1wt % to 7 wt%, the peaks of 450 nm and 480 nm become strong, which is caused by the defects formed in mechanical process, indicating the high rate of combination of photo-induced electron and hole.

Refererces

[1] Yan S C, Li Z S, Zou Z G. Photodegradation Performance of g-C_3N_4 Fabricated by Directly Heating Melamine. *Langmuir.* 2009, 25, 10397-10401.

[2] Zhang Y J, Thomas A, Antonietti M, Wang X C. Activation of Carbon Nitride Solids by Protonation: Morphology Changes, Enhanced Ionic Conductivity, and Photoconduction Experiments. *J. Am. Chem. Soc*. 2009, 131, 50-52.

[3] Liu L, Ma D, Zheng H, Li X J, Cheng M J, Bao X H. Synthesis and Characterization of Microporous Carbon Nitride. *Microporous Mesoporous Mater*. 2008, 110, 216-222.

[4] Yan H J, Yang H X. TiO_2-g-C_3N_4 Composite Materials for Photocatalytic H_2 Evolution under Visible Light Irradiation. *J. Alloys Compd.* 2011, 509, 26-29.

[5] Ge L, Han C C, Liu J. Novel Visible Light-induced g-C_3N_4/Bi_2WO_6 Composite Photocatalysts for Efficient Degradation of Methyl orange. *Appl. Catal. B: Environ*. 2011, 108-109, 100-107.

[6] Cai T J, Yue M, Wang X W, Deng Q. Preparation, Characterization, and Photocatalytic Performance of $NdPW_{12}O_{40}$/TiO_2 Composite. *Catalyst. Chin. J. Catal*. 2007, 28, 10-16.